FILM CONDENSATION ON THE UNDERSIDE OF A HORIZONTAL SURFACE

by

JOSEPH GERSTMANN

B.S., Tufts University

(1962)

SUBMITTED IN PARTIAL FULFILLMENT

OF THE REQUIREMENTS FOR THE

DEGREE OF MASTER OF

SCIENCE

at the

MASSACHUSETTS INSTITUTE OF

TECHNOLOGY

January 1964

Signature of Author .....

Department of Mechanical Engineering, January 20, 1964

Certified by .....

Thesis Supervisor

Accepted by .....

Chairman, Departmental Committee on Graduate Students

FILM CONDENSATION ON THE UNDERSIDE OF A HORIZONTAL SURFACE

Joseph Gerstmann

Submitted to the Department of Mechanical Engineering on January 20, 1964 in partial fulfillment of the requirement for the degree of Master of Science.

ABSTRACT

Heat transfer rates in film condensation on the underside of a horizontal surface are measured experimentally, and the mechanisms of condensation are observed visually and photographically. It is proposed that the characteristic drop dimension is given by the Taylor Instability wavelength and that the film thickness is determined by the radial flow of condensate into a drop. The similarity between the condensation phenomenon and that of film boiling on a horizontal surface is noted, and an equation predicting the heat transfer rate is derived which is similar to that of Berenson's for film boiling. The prediction requires the experimental determination of a constant which is found to be higher than that suggested by Popov. Some curious phenomena of transient formation of condensate film and of the stabilization of the interface by non-condensable gases are discussed.

Thesis Supervisor: Peter Griffith

Title: Associate Professor of Mechanical Engineering

TABLE OF CONTENTS

LIST OF FIGURES

1. INTRODUCTION

At the present time, accurate predictions of film condensation rates on vertical or "near vertical" surfaces under the action of gravity can be made. If the flow is laminar, and there are no surface waves, the Nusselt's analysis (1), or modified forms of it taking into account interfacial shear, agrees quite well with experiment for liquids other than liquid metals. However, as the surface begins to face in the direction of gravity, interfacial forces become of importance, and one must now take into account surface instabilities. To date, there is no precise treatment of the effects of such surface phenomena.

In particular, a case in which interfacial instability plays the predominant role is that of film condensation on the underside of a horizontal surface. Here the film knows no preferred tangential direction, hence it can have only tangential velocities that vary periodically in time and/or space. The characteristic length of the system is not immediately evident as there is no "distance from the leading edge", as there would be for a vertical surface.

In an effort to gain further insight into the problem, we note that, if we were to rotate the condensing surface 180 degrees and reverse the roles played by liquid and vapor, then the condensing system is the same as that of film boiling on the upper side of a horizontal surface. Thus, assuming that the relative magnitudes of the forces involved do not differ

greatly in the two phenomena, we would expect that an analysis which is valid for film boiling will hold for film condensation on a horizontal surface. Of the several correlations available, (2,3,4), that of Berenson (2) appears to agree most closely with experimental data. He suggests that the heat transfer coefficient will be correlated by:

$$\frac{h}{k}\sqrt{\frac{\sigma}{g(\rho-\rho_v)}} = 0.425\left[\frac{g\rho_v(\rho-\rho_v)\Delta H}{\mu_v k_v \Delta T_{SAT}}\left(\frac{\sigma}{g(\rho-\rho_v)}\right)^{3/2}\right]^{1/4} \qquad 1.1$$

In this expression the characteristic length dimension is taken to be the wavelength of fastest growing instability.

To our knowledge, the only other existing correlation is that of Popov (5) in which he suggests that the heat transfer coefficient is given by:

$$\frac{h}{k}\sqrt{\frac{\sigma}{g(\rho-\rho_v)}} = 0.149\left[\frac{g\rho(\rho-\rho_v)\Delta H}{k\mu \Delta T_{SAT}}\left(\frac{\sigma}{g(\rho-\rho_v)}\right)^{3/2}\right]^{1/4} \qquad 1.2$$

We see that, except for the roles played by liquid and vapor, the expression is similar to equation 1.1. Examination of Popov's data shows considerable scatter, and efforts to reproduce it were unsuccessful, although the ¼ power relationship was confirmed.

The object of the present work was to determine the primary mechanism of film condensation on the underside of a horizontal surface and to develop a means of predicting the condensation rate.

2. EXPERIMENTAL PROGRAM

2.1 Experimental Objectives

The two main objectives of the experimental program were to determine the dependence of the heat transfer rate on the temperature difference between the saturated vapor and the condensing surface and to observe the mechanism of condensation so that an analytical model could be formed. In order to cover the widest range of properties, water and Freon 113 were used as condensing fluids as these two differ greatly in their heat of vaporization, thermal conductivity, viscosity, and surface tension. In addition to measuring heat transfer rates and temperatures, visual and photographic observations were made of drop spacing, drop height, and drop departure.

2.2 Experimental Apparatus

Although as the test proceeded several refinements were made on the experimental apparatus, the basic apparatus remained the same. The test chamber consisted of a 12" x 12" x 24" pyrex jar sealed at the top with a 1" x 16" x 16" bakelite plate. At the bottom of the jar were one, two, or four 750 watt hot plate replacement heaters, depending on power requirements. Suspended from the top cover was a 500 ml. graduated beaker with 25 ml. graduations. Above the beaker was a funnel which collected the condensate from the test surface and directed it into the beaker. Tygon tubing led from the beaker to outside the condensing chamber so that the contents of the beaker could be emptied after each run.

The test surface itself consisted of a 5" diameter, 2" thick copper block into which had been cut 1" deep channels to improve the heat transfer effectiveness on the cooling water side (Figure 1). The channeled side was enclosed with a neoprene gasket and a ¼" thick brass plate, to which were connected two lengths of 3/8" pipe through which the cooling water flowed. The lengths of pipe were force-fit through the bakelite cover of the pyrex jar and thus supported the condensing surface. The pipe, sides, and top of the condensing block were wrapped with fiberglass insulation and then covered with a cylindrical shell of molded fiberglass. Three copper-constantan thermocouples were placed in holes drilled into the copper block at points ¼", ½", and 3/4" from the condensing surface. The cooling water was fed from a five-gallon reservoir using a D.C.

centrifugal pump having a maximum capacity of one cubic foot per minute. By varying the voltage across the pump motor, the flow rate could be varied from 25% to its maximum flow rate. By using the same water during a test, the water temperature continually increased, thus providing a continually decreasing temperature difference between the condensing surface and the vapor. Excess vapor was vented from the top of the jar and recondensed by passing it through copper coils inside the cooling water reservoir. The condensing chamber was placed inside a 2' x 2' x 3' constant temperature box which was maintained at constant temperature by two 200 watt thermostatically controlled hair dryers. Both air temperature and vapor temperature were measured with mercury thermometers.

Heat transfer rates were measured by two independent means. The first, and considered the most direct, was by measuring the amount of condensate filling the beaker in a given amount of time. The second was by measuring the temperature gradient on the copper block with the three thermocouples embedded in it. The thermocouple outputs were measured with a Leeds and Northrup K-3 potentiometer.

After a few tests had been run, several deficiencies in the apparatus came to light. Because of its very high thermal conductivity, at low heat fluxes the temperature gradients in the copper block were too small to be measured accurately. Also, the pressure drop in the excess vapor vent was large enough to affect the saturation temperature of the vapor considerably. Furthermore, either because of leaks or porosity in the fiberglass shell covering the insulation, as the insulation heated up,

air escaped into the condensing chamber; and as the insulation cooled down, vapor was drawn into the insulation. Lastly, it appeared that the siphoning of condensate from the graduated beaker affected the reproducibility of the tests.

To correct the first of these deficiencies, a 7" diameter, 0.2" thick plate of #304 stainless steel was soldered onto the copper block and a 5" diameter, 3/8" thick copper plate soldered onto the stainless steel. A thermocouple hole was drilled into the bottom copper plate so that the temperature drop across the stainless steel could be measured (Fig. 2). Thermocouple wells were installed in the inlet and outlet of the coolant side of the condensing block and thermopiles producing ten times the emf of a single copper-constantan thermocouple were installed. To minimize edge effects on the condensing surface, a 5" I.D. 8" O.D. bakelite ring was fitted around the lower copper plate so that its surface was flush with the copper surface. The entire condensing block assembly was then fitted to the bottom of an 8" x 8" brass cylinder rolled from 1/16" brass, and this was attached to the bakelite top with suitable gaskets to prevent leakage. The interior of the brass cylinder was then filled with an expanded polyurethane foam having 99% closed cells to assure minimum vapor absorbtion in the event of any leakage (Fig. 3).

The old condenser coil was replaced with a 24" long, 3" diameter glass column inside of which was approximately 50 feet of ¼' coiled

copper tubing through which cold water circulated. Excess vapor entered at the bottom of the column, condensed on the coils, and then returned to the condensing chamber. The glass column was open at the top, and the vapor in the column was maintained at a high enough velocity so that all non-condensable gases were removed at the top of the column and could not diffuse back into the chamber. The coolant water flow rate was measured with a Fischer-Porter Rotameter. Its calibration curve is presented in Fig. 4.

After the above refinements were made, no further changes became necessary.

2.3 Experimental Procedure

As was mentioned above, preliminary tests indicated that the periodic emptying of the measuring beaker affected the reproducibility of the data. A possible explanation of this is that air was introduced into the system by the siphon. However, as the measurement of condensate was considered the most direct and reliable method of determining the heat transfer rate, it was decided to make simultaneous measurements of amount of condensate, temperature gradient across the stainless steel, and enthalpy increase of the coolant for use as calibration of the temperature gradient measurement and as a check on the coolant enthalpy increase measurement. After the correlation between temperature gradient and heat flux had been completed, the measuring beaker was discarded and heat flux measurements were made only with the thermocouples in the condensing block and in the coolant inlet and outlet.

Of the two fluids used throughout the tests, Freon 113 and water, Freon was the most extensively used. Among the reasons for this choice were its low boiling point, low latent heat, non-flammability, low toxicity, and high density. As the Freon was continually being distilled during a test, maintaining its purity was not a problem. However, after several hours use, the test Freon was redistilled to remove any absorbed water which might raise its boiling temperature.

At the start of a test the constant temperature chamber was turned on to the saturation temperature of the fluid being tested. About two

gallons of the test fluid was poured into the condensing chamber. After the entire system had come to equilibrium at saturation temperature, the heaters at the bottom of the chamber were turned on to maximum power. As Freon vapor is heavier than air, the rising Freon vapor displaced most of the air in front of it with a minimum of diffusion. When the Freon vapor reached the excess vapor condenser, it condensed and returned to the condensing chamber, while any air mixed with the vapor escaped through the top of the condenser. After about an hour of this operation, the chamber was sufficiently free of air for tests to begin. In the case of water vapor, it required five or six hours to rid the system of air.

Normally the tests were started with the coolant fluid at the temperature of melting ice. Some tests, however, were run with a mixture of anti-freeze and water cooled to about -40°F. with dry ice. The coolant was allowed to circulate through the condensing block for several minutes before any data was taken.

Five basic measurements were taken during the tests:

1. Vapor temperature
2. Thermocouple emf across the stainless steel plate
3. Thermocouple emf between the copper condensing surface and the ice bath
4. Thermopile emf between the coolant inlet and outlet
5. Coolant flow rate

From these five measurements two independent determinations of the

heat transfer rate could be made, and the temperature difference between the condensing surface and the saturated vapor determined. The method of calculation is presented in Appendix A.

2.4 Experimental Results

After the changes in the apparatus noted in the preceding section had been completed, the apparatus yielded consistently reproducible data. Tests were run with Freon 113 at atmospheric pressure and at temperature differences ranging between 10 and 60 degrees F. The data from these tests is presented in Appendix B, and the results plotted in Figure 5 showing Q/A plotted versus $T_{sat} - T_{wall}$. The tests run with water presented some difficulty as the condensate film refused to wet the surface of the plate. At first, the copper was thoroughly washed with Alconox detergent, rinsed, dried, and then placed in the condensing chamber. When this failed to produce complete filmwise condensation, the copper surface was washed, rinsed, dried, and then sanded down with emery cloth. After using a very fine emery cloth, the plate was polished with #00 steel wool and then repeatedly washed with distilled water. The condensing chamber was heated until filled with steam, and then, while still wet, the condensing surface was set inside the chamber. After a few minutes the surface was completely wet with condensate (Fig. 6). After several hours, when the chamber was free of air, the data presented in Appendix B was taken. Figure 7 shows Q/A plotted versus $T_{sat} - T_{wall}$ for this test.

During the above tests, photographs and visual observations of the condensing surface were made. The condensate film was made up of many "cosine shaped" drops apparently randomly arrayed. Except for the fact

that the surface of the plate was everywhere "wet", the film thickness appeared to go to zero in the region between drops. Although no attempts were made to time the life of a drop, it was noted that at high heat fluxes the drops had shorter lifetimes than at low heat fluxes. The drops did not stay in one place but meandered about in areas about the order of a few drop diameters. Occasionally, at low heat fluxes, drops would collide on the surface and coalesce. When a drop left the surface, a new one would form in its place, although occasionally a drop would form where there had not been one previously. The size and shape of the drops did not appear to vary with the heat flux.

Before the reflux condenser was used, it appeared that the total number of drops on the surface varied with heat flux. At the time it was not known that air was present in the chamber. When the reflux condenser was added to the system, the number of drops gradually increased as the air was bled from the chamber. Figure 8 shows the condensing surface first with no air present and then after a small amount of air had been blown into the chamber.

Apparently, the presence of a non-condensable gas has resulted in a partial stabilization of the film. As there is a bulk motion of vapor towards the interface, the vapor must diffuse through the gas; hence there must be a concentration gradient. This results in a reduction in the partial pressure of the vapor near the interface; hence the local saturation temperature of the vapor decreases. This decreases the

temperature drop across the film and results in a lower heat transfer rate. If we consider a uniformly thick section of film and apply a slight depression locally, the heat transfer rate will increase in the depressed region. If, however, there are non-condensables present, the increased heat transfer will increase the local concentration of non-condensables, thus lowering the temperature of the interface. The resulting gradient in temperature along the interface results in a gradient in surface tension from the depressed region to the thicker film region. This gradient in surface tension must be balanced by a discontinuity in shear stress across the interface. The shear stress results in a flow of condensate towards the depression, thus ironing out the depression. A similar argument will show that an elevation in film thickness also tends to be ironed out. Apparently, therefore, not only does the presence of a non-condensable gas reduce the heat transfer rate by lowering the partial pressure of the vapor at the condensing surface, but also by stabilizing the film, hence reducing the rate at which condensate is removed from the surface.

The question arose as to whether the heat transfer rate would change appreciably if the plate were slightly tilted. To test this the plate was slightly tilted so that all the drops ran off to one side (but did not form "ridges" or waves). With the surface tilted about five to seven degrees, there was no measurable change in the heat transfer rate. As, when the plate is horizontal, the drops wander about the surface, one

might expect that there will be little change if all the drops move in the same direction, as the change in the downward body force in the film is proportional to the cosine of the angle of tilt.

One of the basic assumptions regarding the validity of the data in truly representing an infinite surface is that the presence of the boundary is not felt by the film except right at the boundary. Otherwise the characteristic dimension of the system might be taken as the diameter of the plate. Some insight into the validity of this assumption might be gained from the following experiment. Vapor was condensed on the copper surface until almost no more condensation was taking place. Then the power to the heaters was decreased so that less vapor was generated. As a result, the pressure in the chamber decreased slightly so that the saturation temperature also decreased. As the copper condensing surface was now slightly warmer than saturation temperature, the liquid film on it evaporated and the surface became dry. Then the power to the heaters was once again increased, producing a rise in pressure in the chamber, and the transient formation of the film was photographed. Figure 9 shows a typical sequence spanning about twenty seconds. Evidently, the boundary of the plate has a profound effect on the initial formation pattern of the drops. However, by the time the last ring of drops has formed near the center of the plate, several of the drops near the edge of the plate have already fallen and the drop spacing is already becoming quite random. Thus, we may conclude that the initial conditions and the details of the boundaries soon have little or no effect on the mechanism

of drop formation.

3. THEORETICAL INVESTIGATION

3.1 Heat Transfer Analysis of a Single Drop

From the observations of the previous section, it is obvious that if the mechanism of heat transfer is conduction through the condensate film then, as the film in the region between drops is much thinner than the height of the drops, the bulk of the heat transfer ought to occur in this region. However, as the transformation of vapor into liquid is a measure of the magnitude of the heat transfer rate, then, if the "thin film" region is to remain thin, the condensate must be removed by a flow into the drops. Thus if one had to separate the area about a drop into regions, he might describe the central region as a region of "thick" film through which little heat is transferred, and the surrounding area as one of "thin" film through which the bulk of the heat transfer occurs. Then, in order to predict the heat transfer rate, it would be sufficient to calculate only the heat transferred through the region of thin film.

The actual shape of a pendant drop is shown in Figure 10a. We shall approximate this shape by dividing the drop into the two regions described above, as shown in Figure 10b. The central part of the drop is assumed to be a hemisphere of radium r_i, while the thin film region is described by $\delta = a/r$, where a is to be determined. The following are the assumptions to be used in the analysis:

1. The condensate flows radially into the drop. Near the outer regions of the film, there may be tangential components but they should be small compared to the radial component.

2. The flow is laminar. Calculation of the Reynolds Number shows this to be true except for extremely large temperature differences.

3. The component of velocity in the y-direction is negligible compared to the radial component. This should be true if the slope of the interface is small (i.e., in the thin film region).

4. The curvature of the film in the thin film region is much less than at the center of the drop. Examination of Figure 10 shows this to be the case.

5. The momentum forces are small compared to viscous forces in the region of thin film. The Reynolds Number calculation shows this to be an excellent approximation.

6. The vapor exerts negligible drag on the film. This should be true if the vapor is stagnant and if the velocities in the film are small.

7. The vapor velocity is zero at $r = r_o$. This would not be true for a single drop but must be true for multiple drops from symmetry considerations.

8. Heat is transferred through the condensate film by conduction.

9. The vapor is at saturation temperature.

Under the conditions stated above the momentum equation for two dimensional flow becomes

$$\frac{\partial p}{\partial r} = \mu \frac{\partial^2 V_r}{\partial y^2}$$

$$V_r(0) = 0 \; ; \; \left(\frac{\partial V_r}{\partial y}\right)_\delta = 0 \qquad 3.1$$

The pressure, p, is in general a function of both r and y, but as the y-direction velocity is taken to be zero, $\frac{\partial p}{\partial r}$ is a function of r alone. Thus we can multiply by dy and integrate to obtain

$$\delta \frac{\partial p}{\partial r} = -\mu \left(\frac{\partial V_r}{\partial y}\right)_0 \qquad 3.2$$

If we now assume a velocity profile which satisfies the boundary conditions in 3.1, such as

$$\frac{V_r}{V_\delta} = 2\frac{y}{\delta} - \left(\frac{y}{\delta}\right)^2 \qquad 3.3$$

and perform the indicated differentiation in equation 3.2 we obtain

$$\delta \frac{dp}{dr} = -2\mu \frac{V_\delta}{\delta} \qquad 3.4$$

An energy balance taken between r_o and r requires that

$$\int_o^r \frac{K \Delta T_{SAT}}{\delta} 2\pi r\, dr = 2\pi r \delta \bar{V}_r \rho \Delta H \qquad 3.5$$

Taking the average of the velocity described by 3.3, we find

$$\bar{V}_r = \frac{2}{3} V_\delta \qquad 3.6$$

and in accordance with the assumed shape of the thin film region of the drop

$$\delta = a/r \qquad 3.7$$

Integration of 3.5 results in

$$V_\delta = \frac{k \Delta T_{SAT} (r^3 - r_o^3)}{2 \rho a^2 \Delta H} \qquad 3.8$$

Using this result, we now integrate equation 3.4 between r_o and r_i to obtain

$$p_o - p_i = \frac{k\mu \Delta T_{SAT}}{3\rho a^4 \Delta H}\left(r_o^3 - r_i^3\right)^2 \qquad 3.9$$

But if $\delta \ll r_i$, then

$$p_o - p_i = (\rho - \rho_v) g r_i - 2\sigma / r_i \qquad 3.10$$

Therefore, upon re-arrangement 3.9 results in

$$a^4 = \frac{k\mu \Delta T_{SAT}}{3\rho(\rho-\rho_v) g \Delta H} \cdot \frac{r_i\left(r_o^3 - r_i^3\right)^2}{r_i^2 - 2\sigma / g(\rho-\rho_v)} \qquad 3.11$$

If we define the average heat transfer coefficient, h, as

$$h \equiv \frac{Q/A}{\Delta T_{SAT}} = \frac{1}{\pi r_o^2}\int_0^{r_o} \frac{k}{\delta} 2\pi r \, dr \qquad 3.12$$

then we arrive at

$$h = \frac{2}{3}\left\{\frac{k^3 \rho(\rho-\rho_v) g \Delta H}{\mu \Delta T_{SAT}}\right\}^{1/4}\left\{\frac{r_o^4\left(r_i^2 - 2\sigma / g(\rho-\rho_v)\right)}{r_i\left(r_o^3 - r_i^3\right)^2}\right\}^{1/4} \qquad 3.13$$

With this result, all that remains is to evaluate r_o and r_i.

3.2 Determination of Characteristic Drop Dimension

We have derived in the previous section an expression of relating the heat transfer coefficient to fluid properties, temperature difference, and drop dimensions. It is now necessary to analyze the hydrodynamics of the film as a whole in order to determine those drop dimensions. To determine the bubble dimensions in film boiling, Berenson used Taylor's instability analysis (6) in which he assumed a two-dimensional disturbance given by

$$\delta = \delta_0 e^{bt} \cos kr \qquad 3.14$$

This results in a relationship between fluid properties, fluid depth, fluid velocity, and wave speed given by

$$k\rho_l (V_l - c)^2 \coth(ka_l) + k\rho_v (V_v - c)^2 \coth(ka_v) = \sigma k^2 - g(\rho - \rho_v) \qquad 3.15$$

where k is the wave number, and a_l and a_v refer to the liquid and vapor depths, respectively.

If we neglect the liquid and vapor velocities compared to the wave speed, c, we find for the most unstable wave length that

$$\lambda = 2\pi\eta \sqrt{\frac{\sigma}{g(\rho - \rho_v)}} \qquad 3.16$$

where η lies between $\sqrt{2}$ and $\sqrt{3}$ depending on whether the wavelength is much longer than or shorter than the unperturbed liquid depth.

Maxwell (7) showed that for an interface contained in a rectangular

slit, the initial unstable wavelength was given by

$$\lambda = 2\pi\eta\sqrt{\frac{\sigma}{g(\rho-\rho_v)}}\,; \qquad \eta = 1/2 \tag{3.17}$$

while for an interface contained in a circular orifice, η was equal to 1.22. These analyses are all similar in that the wavelength is proportional to the square root of a ratio of surface to body forces given by $\sigma/g(\rho-\rho_v)$. For the general case of a three-dimensional disturbance, Melcher (8) shows that, if the disturbance is of the form,

$$\delta = \delta_0 \, Re\left\{e^{i(\omega t - k_2 x_2 - k_3 x_3)}\right\} \tag{3.18}$$

then the frequency is given by

$$\omega^2 = k^2\left(V_c^2 - V_g^2\right)$$

$$k^2 = k_2^2 + k_3^2$$

$$V_c^2 = \frac{\sigma k}{\rho_{eq}} \qquad V_g^2 = \frac{g(\rho-\rho_v)}{k\rho_{eq}}$$

$$\rho_{eq} = \rho\coth(ka_L) + \rho_v\coth(ka_v) \tag{3.19}$$

If ω^2 is negative, then the interface is unstable, and the value of the most unstable wavelength is the same as that given by equation 3.16. In the case of a two-dimensional sinosoidal disturbance as in 3.14, λ is simply the distance between wave crests. However, for the case of a three-dimensional disturbance, the relationship between λ and the distance tween peaks and troughs is more complicated, as there is

yet one more unknown, the ratio of k_2 to k_3. If the drops are arranged in a square lattice, then k_2 equals k_3 and λ corresponds to the shortest distance between drops. If the drops are arranged in hexagonal lattices, then k_2 equals $\sqrt{3}k_3$ and λ corresponds to 0.796 times the shortest distance between drops. It is evident, therefore, that the determination of drop spacing requires a knowledge of the arrangement of the drops. Thus the most that we can conclude is that the drop spacing is given by

$$r_o = 2\pi B\sqrt{\frac{\sigma}{g(\rho-\rho_v)}} \qquad 3.20$$

where B is a function of the drop pattern.

In the drop model we have chosen we note that r_i corresponds not only to the maximum height of the drop but also to one of the limits of integration for determining the extent of the region of thin film. The value of the average heat transfer coefficient, h, is, therefore, doubly sensitive to the value of r_i. This is one of the inherent limitations of the model used.

There exist in the literature many predictions of the value of this radius (references 2, 9, 10). Although the predictions differ substantially in the value of r_i, they all have in common the fact that r_i may be expressed as a constant times $\sqrt{\frac{\sigma}{g(\rho-\rho_v)}}$. Thus the entire quantity in the second brackets in equation 3.13 may be expressed as a constant times r_o^{-1}. Defining a Nusselt Number based on drop spacing, we find

$$\frac{h}{k}\sqrt{\frac{\sigma}{g(\rho-\rho_v)}} = C\left[\frac{g\rho(\rho-\rho_v)\Delta H}{k\mu\Delta T_{SAT}}\left(\frac{\sigma}{g(\rho-\rho_v)}\right)^{3/2}\right]^{1/4} \qquad 3.21$$

where C is made up of the undetermined constants and is to be fixed by experimental data. It is seen that this equation is identical to Berenson's equation for the heat transfer rate for film boiling with liquid properties replaced by vapor properties.

4. CONCLUSIONS

If we plot the data for Freon 113 and water from Figures 6 and 8 in terms of the dimensionless parameters of equation 3.25, the value of C is found to be 0.26. (Fig. 11) This differs considerably from the value of 0.149 suggested by Popov (5), but examination of his data shows considerable scatter which suggests that perhaps non-condensable gases were present. Therefore, for film condensation on the underside of a horizontal surface the heat transfer coefficient will be predicted by the following relationship.

$$\frac{h}{k}\sqrt{\frac{\sigma}{g(\rho-\rho_v)}} = 0.26\left[\frac{g\rho(\rho-\rho_v)\Delta H}{K\Delta T_{sat}\mu}\left(\frac{\sigma}{g(\rho-\rho_v)}\right)^{3/2}\right]^{1/4} \qquad 4.1$$

This equation should be valid in the absence of non-condensable gases and if the condensing vapor exerts no shear on the interface. As the analysis assumes that viscous forces predominate over inertial forces, it is restricted to values of $k\Delta T/\mu\Delta H$ less than unity. As the phenomenon does not change appreciably for small angles of tilt, equation 4.1 should still be valid as long as the cosine of the angle of tilt is still close to unity. However, the substitution of g cos θ, where θ is the angle of tilt, for g in equation 4.1 should not be expected to correlate results when θ becomes large, as the film thickness will no longer be periodic in space but will vary with distance from the upper edge.

REFERENCES

1. Nusselt, W., Z. ver Deut. Ing., 60, 541 (1916).

2. Berenson, P. J., "Transition Boiling Heat Transfer from a Horizontal Surface", Technical Report No. 17, Division of Sponsored Research, M.I.T., March 1960.

3. Zuber, N., and M. Tribus, "Further Remarks on the Stability of Boiling Heat Transfer", Report No. 58-5, Dept. of Engr., U.C.L.A., January 1958.

4. Bromley, L. A., et al., Ind. Eng. Chem., 45, 2639 (1953).

5. Popov, V. D., Trudy K.T.I.P.P. im A. I. Mikoyana, 11, 87 (1951).

6. Taylor, G. I., "The Instability of Liquid Surfaces When Accelerated in a Direction Perpendicular to Their Plane", Proc. Royal Soc. London, A-202, 81 (1950).

7. Maxwell, J. C., Encyclopaedia Britannica, 11th. Ed., 5, 273 (1910).

8. Melcher, J. R., Field Coupled Surface Waves, M.I.T. Press, Cambridge, Mass. (1963).

9. Borishansky, V. M., "Heat Transfer to a Liquid Freely Flowing Over a Surface Heated to a Temperature Above the Boiling Point", Problems of Heat Transfer During a Change of State, S.S. Kutateladze, (1953) AEC-tr-3405.

10. Fritz, W., Z. Physik, 36, 379 (1935).

NOMENCLATURE

a	Constant product of radius and film thickness, (ft^2)
a_l	Average film thickness, (ft)
a_v	Average vapor depth, (ft)
A	Area of condensing surface, (ft^2)
b	Growth coefficient, (1/t)
B	Constant, (Eqn. 3.20)
c	Wave Speed, (ft/hr)
C	Constant, (Eqn. 3.21)
C_p	Specific heat, (BTU/lbm-^oF)*
E_w	Thermocouple output between condensing surface and ice bath, (μv)
ΔE_{io}	Thermopile output between coolant inlet and outlet, (μv)
ΔE_{ss}	Thermocouple output across stainless steel plate, (μv)
g	Acceleration of gravity, (ft/hr^2)
h	Heat transfer coefficient, (BTU/hr-ft^2-^oF)
h_{fg}	Heat of vaporization, (BTU/lbm)
h_{io}	Heat transfer coefficient based on ΔE_{io}, (BTU/hr-ft^2-^oF)
h_{ss}	Heat transfer coefficient based on ΔE_{ss}, (BTU/hr-ft^2-^oF)
ΔH	Decrease in specific enthalpy of vapor in its transformation to subcooled liquid, (BTU/lbm)
I	Enthalpy, (BTU)
k	Thermal conductivity, (BTU/hr-ft-^oF); wave number, equal to $2\pi/\lambda$, (1/ft)

* In dynamical equations containing both lbm and lbf, lbm must be divided by $g_0 = 4.73 \times 10^8 \frac{\text{lbm-ft}}{\text{lbf-hr}^2} = 1$

$\dot{m}$	Mass flow rate of coolant, (lbm/hr)
p	Pressure, (lbf/ft^2)
Q	Heat transfer rate, (BTU/hr)
Q/A_{io}	Heat transfer rate based on ΔE_{io}, ($BTU/hr\text{-}ft^2$)
Q/A_{ss}	Heat transfer rate based on ΔE_{ss}, ($BTU/hr\text{-}ft^2$)
r	Length coordinate, (ft)
r_i	Inner drop radius, (ft)
r_o	Outer drop radius, (ft)
t	Time, (hr)
ΔT_{sat}	Temperature difference between solid surface and saturated vapor, (^oF)
V_r	Radial velocity, (ft/hr)
V_δ	Radial velocity at interface, (ft/hr)
$\bar{V}_r$	Average radial velocity, (ft/hr)
$\mathcal{V}$	Volume of condensate in a given sample, (ft^3)
x	Length coordinate, (ft)
y	Length coordinate, (ft)

Greek Letters

β	Constant, (Eqn. A-1)
δ	Film thickness, (ft)
η	Constant, (Eqn. 3.16)
θ	Angle of tilt
λ	Wavelength, (ft)
μ	Viscosity, (lbm/hr-ft)
ρ	Density, (lbm/ft^3)

σ	Surface tension, (lbf/ft)
ω	Angular frequency, (1/hr)

Subscripts

v	Vapor*
1,2,3	Mutually orthogonal directions

*Properties unsubscripted refer to the liquid.

APPENDIX A

Calculation of Heat Transfer Rates

There were three methods used for measurement of heat transfer rates. The independent methods were measurement of amount of condensate and measurement of the rate of enthalpy increase of the coolant. The dependent method was the measurement of the temperature drop in the condensing block.

The First Law requires that the heat transferred by conduction through the condensate film be equal to the enthalpy decrease of the vapor in its transformation into sub-cooled liquid. This change in enthalpy is given by

$$\Delta I = \rho \mathcal{V} \left(h_{fg} + \beta C_p \Delta T_{SAT} \right) \qquad \text{A-1}$$

where β is of order 0.5. As the condensate leaves the condensing surface and falls into the measuring beaker it is sub-cooled by an amount $\beta \Delta T_{SAT}$. Thus it is possible that the condensate in the beaker will increase its amount by

$$\frac{\Delta \mathcal{V}}{\mathcal{V}} = \frac{\beta C_p \Delta T_{SAT}}{h_{fg}} \qquad \text{A-2}$$

We must, therefore, deduct from the measured amount of condensate an amount equal to $\Delta \mathcal{V}$. With this correction the heat balance becomes

$$\Delta I = \rho \mathcal{V} h_{fg} \qquad \text{A-3}$$

This equation will be in error by the amount of heat that is transferred through the sides of the beaker, thereby not adding to the condensate in the beaker. For a ΔT_{sat} of 50°F. for Freon 113, this will introduce an error of not more than 10%; for water, not more than 2.5%. Using equation A-3, the heat transfer rate becomes

$$Q/A = \frac{\rho V h_{fg}}{A t} \qquad \text{A-4}$$

where t is the time to collect the given volume of condensate.

Assuming that all the heat transferred through the copper condensing surface goes into the cooling water, then the heat transfer rate is equal to

$$\frac{Q}{A} = \frac{\dot{m} C_{P_{H_2O}} \Delta T_{io}}{A} \qquad \text{A-5}$$

where $\dot{m}$ is the mass flow rate of the cooling water and ΔT_{io} is the temperature rise of the cooling water between the inlet and outlet of the condensing block.

Using equations A-4 and A-5 we have two independent methods of determining the heat transfer rate. The dependent method, which was used mainly as a check on the other two methods, consisted of calibrating the temperature drop across the stainless steel with the heat transfer rate as measured by collection of condensate.

APPENDIX B

Test Data

The test data is given in terms of copper-constantan thermocouple outputs in microvolts, and flow rate readings in terms of scale divisions of the particular rotameter used. Its calibration curve is given in Figure 4. Also presented are the calculated ΔT_{sat}, heat transfer rates, and heat transfer coefficients. In run #1, anti-freeze was used as the coolant, so the only measurement of heat transfer rate was by the temperature drop across the stainless steel plate, ΔE_{ss}. E_w refers to the emf of the thermocouple in the copper condensing surface and represents the surface temperature of the plate. Where two measurements of heat transfer rate have been made, the data is plotted as a line between the two points in Figures 5 and 7. Note that ΔE_{io} refers to the output of a differential thermopile consisting of ten copper-constantan junctions at each leg.

Table 1

TEST DATA

Test Fluid: Freon 113; Vapor Temperature 118.5°F

Run: 1 Date: 3/5/63

Point #	E_w μv.	ΔE_{ss} μv.	T_{sat} °F	Q/A_{ss} BTU/ft²-hr	h_{ss} BTU/ft²-hr-°F
1	640	1187	57.5	8439	146.7
2	615	1182	58	8404	144.9
3	603	1175	59	8354	141.6
4	597	1175	59.5	8354	140.4
5	564	1131	61	8041	131.8
6	597	1161	59.5	8255	138.7
7	599	1178	59.5	8375	140.7
8	590	1178	59.5	8375	140.7
9	585	1180	60	8390	139.8
10	577	1175	60.5	8354	138.1
11	604	1149	59	8169	138.4
12	621	1126	58	8006	138.0
13	687	1081	55	7757	141.0
14	750	1031	52.5	7330	139.6
15	854	955	47.5	6790	142.9
16	865	942	47	6697	142.5
17	890	919	46	6534	142.0
18	931	895	44.5	6367	143.1
19	976	850	42	6043	143.9
20	1065	788	38.5	5002	145.5
21	1137	732	35	5206	148.7
22	1165	713	34	4070	149.1
23	1182	704	33	5005	151.6
24	1275	648	28.5	4608	161.7
25	1300	626	28	4451	158.9
26	1338	593	26	4216	162.1
27	1383	555	24	3946	164.4
28	1415	527	23	3747	162.9
29	1455	500	21	3555	169.3
30	1476	473	20.5	3363	164.1
31	1502	448	19	3185	167.6
32	1519	432	18.5	3071	166
33	1538	418	17.5	2971	169.7
34	1555	405	17	2880	169.4
35	1611	350	14.5	2488	171.6

Table 2

TEST DATA

Test Fluid: Freon 113; Vapor temperature 117°F

Run: 2 Date: 4/4/63

Point #	E_w μv.	ΔE_{ss} μv.	ΔE_{io} μv.	$\dot{m}$ -	$(Q/A)_{io}$ BTU/ft²-hr	$(Q/A)_{ss}$ BTU/ft²-hr	ΔT_{sat} °F	h_{io} BTU/ft²-hr-°F	h_{ss} BTU/ft²-hr-°F
1	913	740	154	24	6900	6360	43.5	159	146
2	925	747	151	23.8	6760	6420	43	155	149
3	920	745	149	23.5	6680	6410	43	155	149
4	930	748	149	23	6680	6430	42.5	157	151
5	933	748	149	23	6680	6430	42.5	157	151
6	938	736	140	22.5	6250	6330	42	149	151
7	955	725	143	22.5	6390	6240	41.5	154	150
8	978	705	126	29	6050	6050	40.5	150	150
9	997	696	119	29	5710	5980	40	143	150
10	1028	678	115	28	5440	5820	38.5	141	151
11	1161	600	105	27	4960	5160	32.5	153	158
12	1176	590	104	26.5	4570	5070	32	143	158
13	1258	530	98	24	4510	4550	28	161	163
14	1265	526	96	24	4420	4510	28	158	161
15	1323	493	90	24.6	4160	4150	25.5	163	163
16	1347	487	89	24	4110	4090	24.5	168	167
17	1353	474	90	19.8	4070	3950	24	169	164

Table 3

TEST DATA

Test Fluid: Water; Vapor Temperature 212°F

Run: 3

Point #	E_w $\mu v.$	ΔE_{ss} $\mu v.$	ΔE_{io} $\mu v.$	$\dot{m}$ -	$(Q/A)_{ss}$ $\frac{BTU}{ft^2\text{-}hr}$	$(Q/A)_{io}$ $\frac{BTU}{ft^2\text{-}hr}$	ΔT_{sat} °F	h_{ss} $\frac{BTU}{ft^2\text{-}hr\text{-}^oF}$	h_{io} $\frac{BTU}{ft^2\text{-}hr\text{-}^oF}$
1	3869	2440	340	55.5	19500	21400	15.8	1232	1352
2	3866	2396	341	55.5	19150	21450	15.9	1204	1348
3	3880	2497	355	55.5	20000	22300	15.4	1299	1448
4	3887	2605	373	55.5	20900	23450	15	1391	1562
5	3875	2618	373	55.5	21000	23450	15.6	1344	1503
6	3880	2494	360	55	20300	22550	15.4	1318	1464
7	3878	2438	357	55	19550	22450	15.5	1262	1448
8	3890	2406	352	55	19200	22100	15.0	1281	1473
9	3895	2391	345	55	19100	21700	14.8	1290	1465
10	3885	2337	337	55	18700	21100	15.2	1218	1388
11	3883	2303	337	55	18400	21100	15.3	1201	1380
12	3892	2276	331	55	18200	20800	14.9	1221	1397
13	3905	2216	325	55	17750	20450	14.4	1231	1419
14	3913	2195	328	55	17600	20650	14	1257	1474
15	3924	2160	320	55	17300	20100	13.6	1273	1478
16	3928	2140	314	55	17100	19750	13.5	1267	1462
17	3931	2125	312	55	17000	19600	13.4	1269	1463
18	3926	2080	307	55	16700	19300	13.6	1228	1419
19	3940	2038	301	55	16300	18950	13.1	1245	1446
20	3951	2018	300	55	16200	18850	12.6	1286	1494
21	3954	2010	292	55	16100	18400	12.5	1288	1471
22	3973	1963	256	55	15700	18000	11.8	1331	1527
23	3977	1920	281	55	15400	17650	11.6	1327	1521
24	3986	1906	277	55	15250	17450	11.3	1352	1543
25	3995	1867	268	55	14950	16850	10.9	1373	1545
26	3998	1826	270	55	14600	17000	10.8	1352	1574

Table 4

FLUID PROPERTIES

FREON 113

Vapor Density, lbm/ft^3(1 atm,118°F)	0.4649
Liquid Density, lbm/ft^3 (1 atm)	$103.555-0.07126T-0.0000636T^2$ (T,$^\circ$F)
Boiling Point, $^\circ$F (1 atm)	117.6
Critical Temperature, $^\circ$F	417.4
Critical Pressure, psia	495
Liquid viscosity, cp	
(40°F)	0.876
(60°F)	0.747
(80°F)	0.646
(100°F)	0.564
(120°F)	0.497
(140°F)	0.442
(160°F)	0.395
Liquid Conductivity,BTU/hr-ft-$^\circ$F	
(-4°F)	0.048
(68°F)	0.043
Surface Tension,lbf/ft	
(40°F)	0.00145
(60°F)	0.00136
(80°F)	0.00126
(100°F)	0.00118
(120°F)	0.00109
Heat of Vaporization,BTU/lbm	
(110°F)	63.71
(114°F)	63.40
(118°F)	63.09
(122°F)	62.78
Liquid Specific Heat,BTU/lbm-$^\circ$F	0.225

WATER AT 200°F

Liquid Density,lbm/ft^3	60.1
Heat of Vaporization,BTU/lbm	978
Specific Heat,BTU/lbm-$^\circ$F	1.00
Thermal Conductivity,BTU/hr-ft-$^\circ$F	0.394
Viscosity,lbm/hr-ft	0.74
Surface Tension,lbf/ft	0.0042

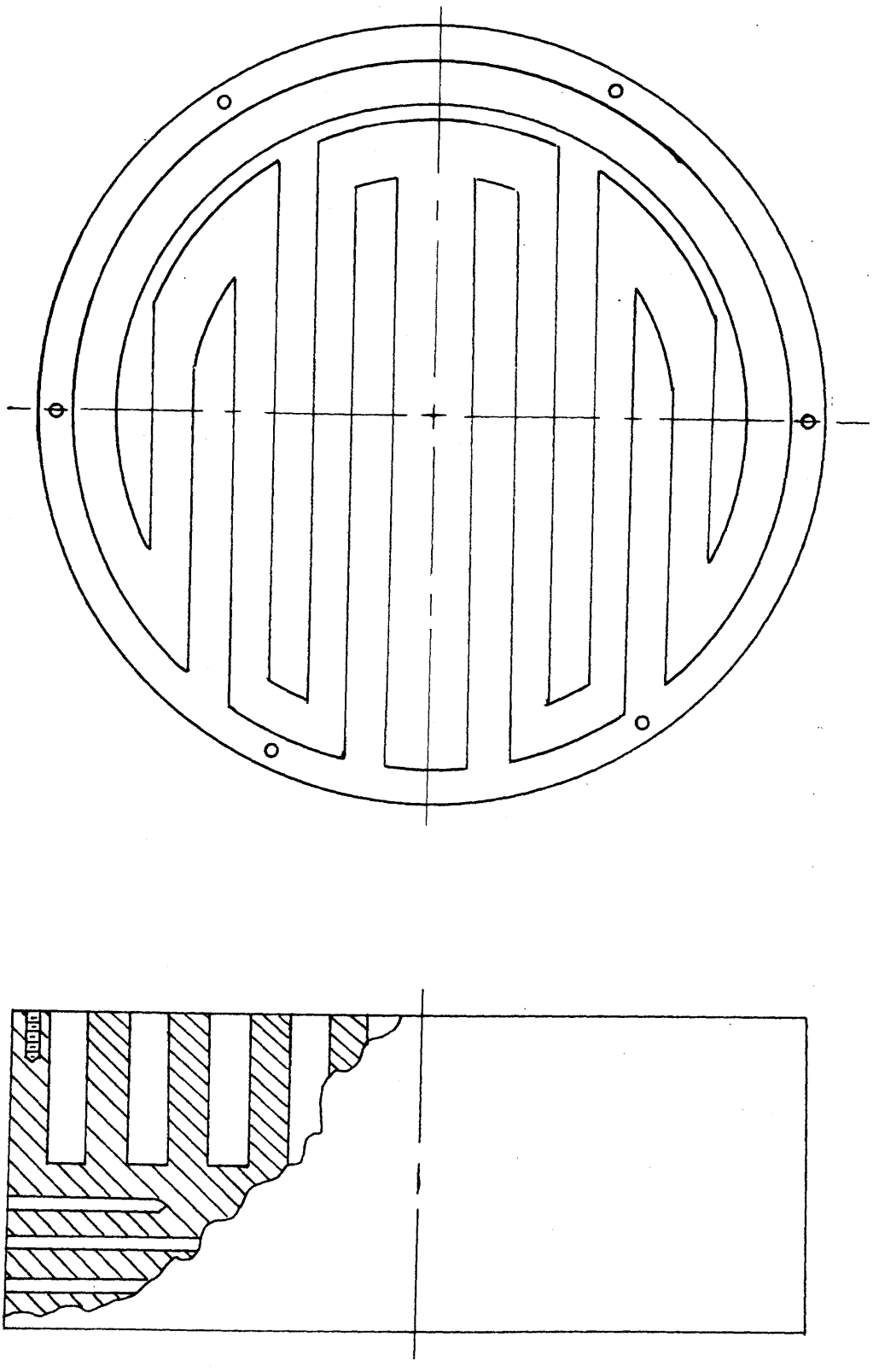

Fig. 1- Copper condensing block

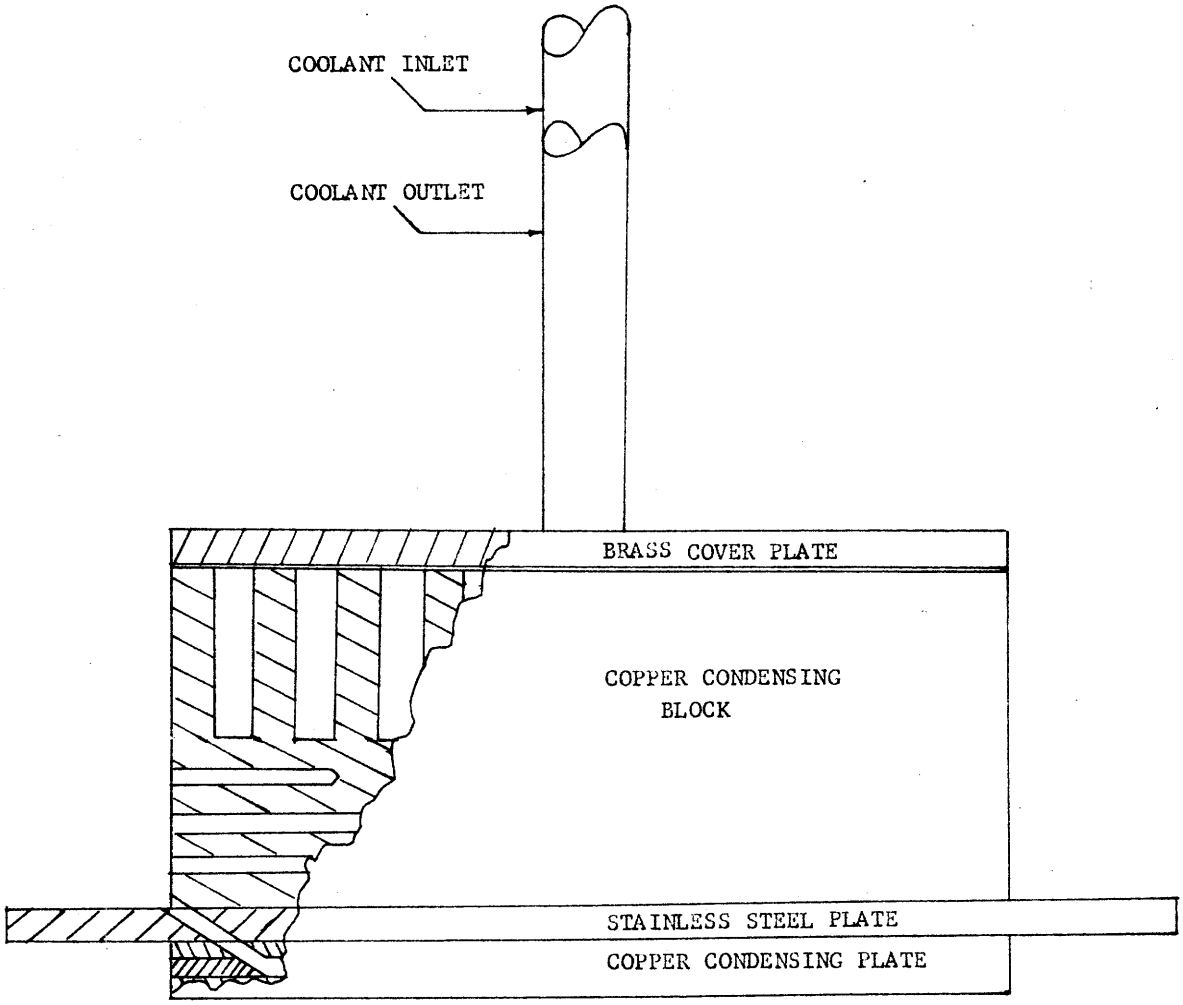

Fig. 2- Condenser Assembly

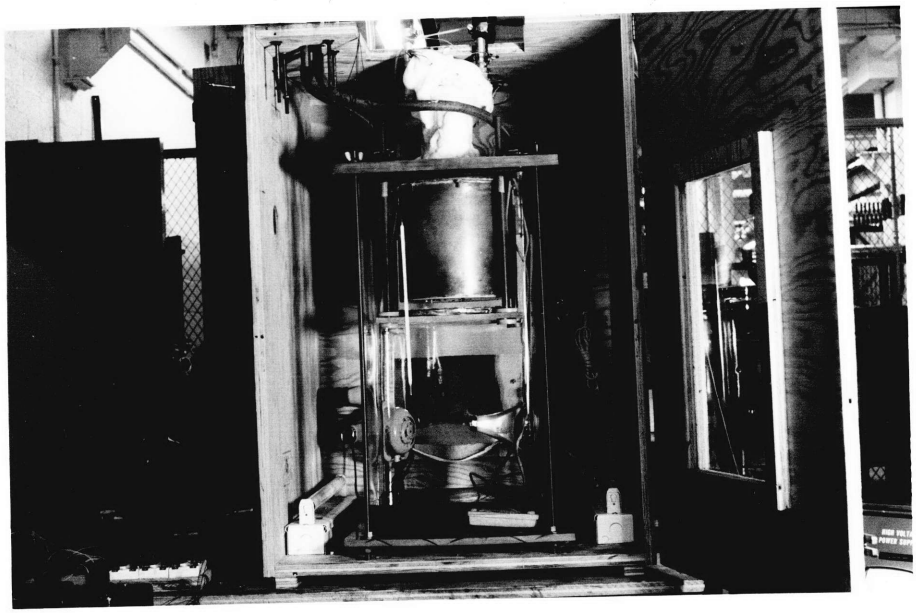

Figure 3 Test Section

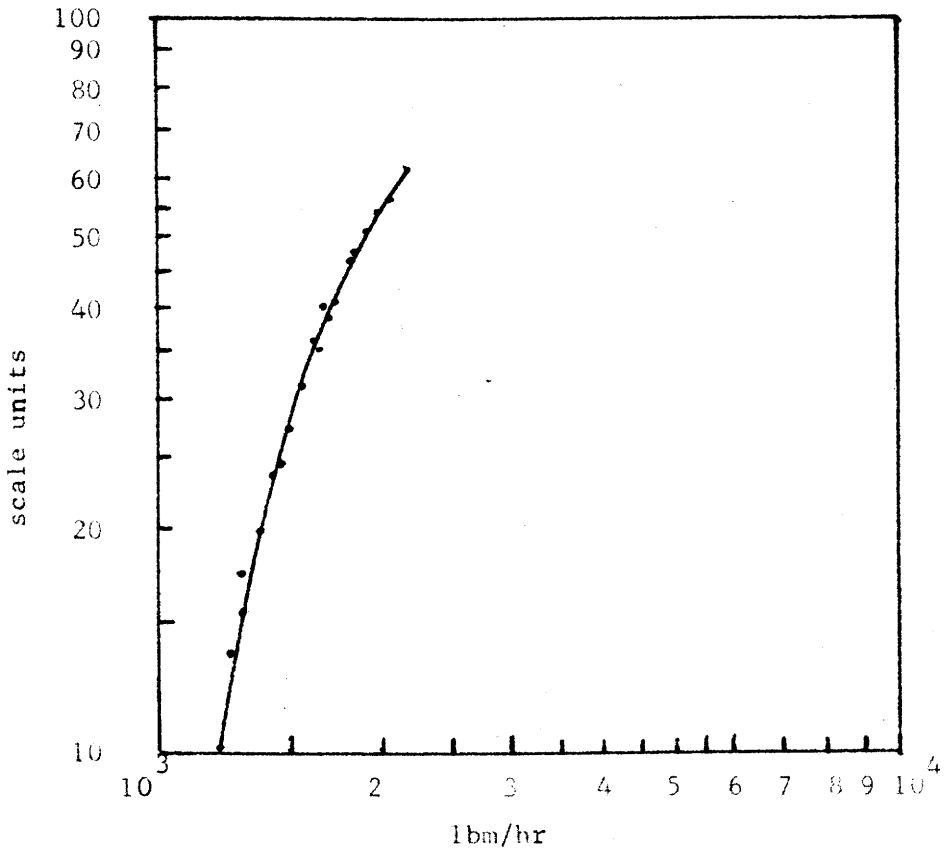

Fig. 4- Rotameter calibration curve
for water at 60° F.

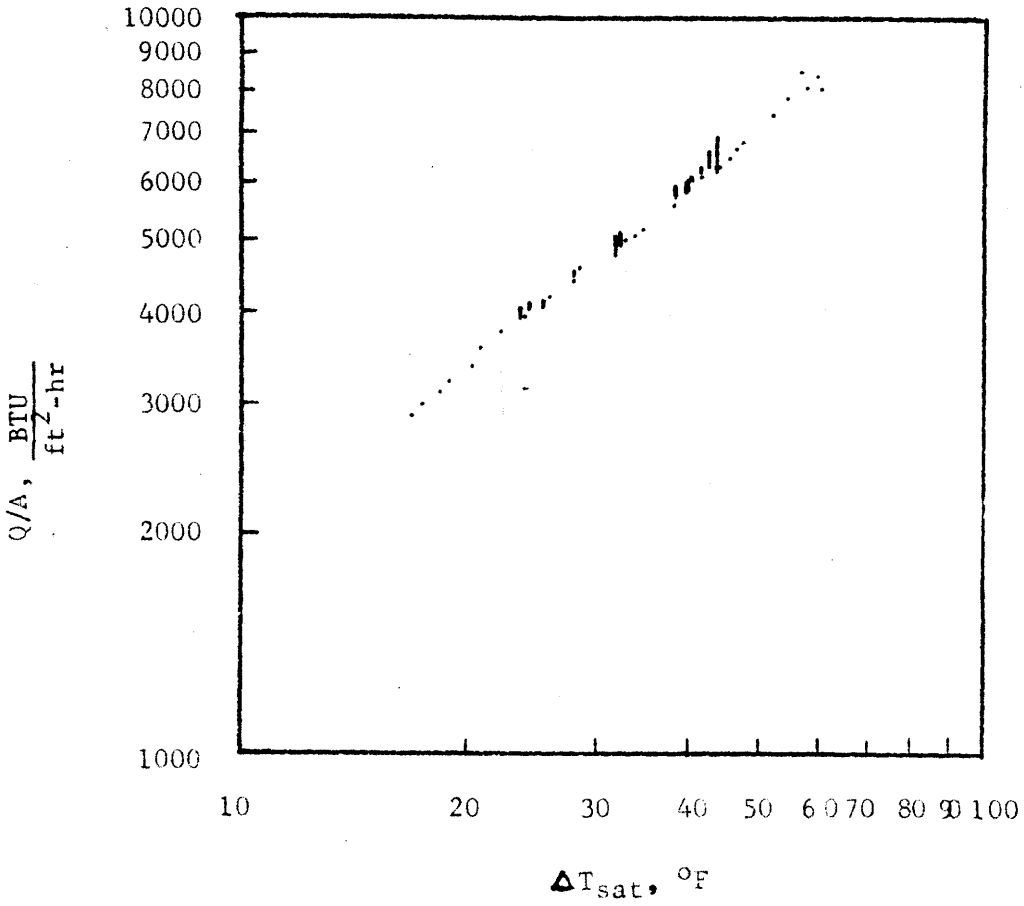

Fig. 5- Q/A versus ΔT_{sat} for Freon 113 at atmospheric pressure

Figure 6 Water Condensing on a 5" Diameter Plate

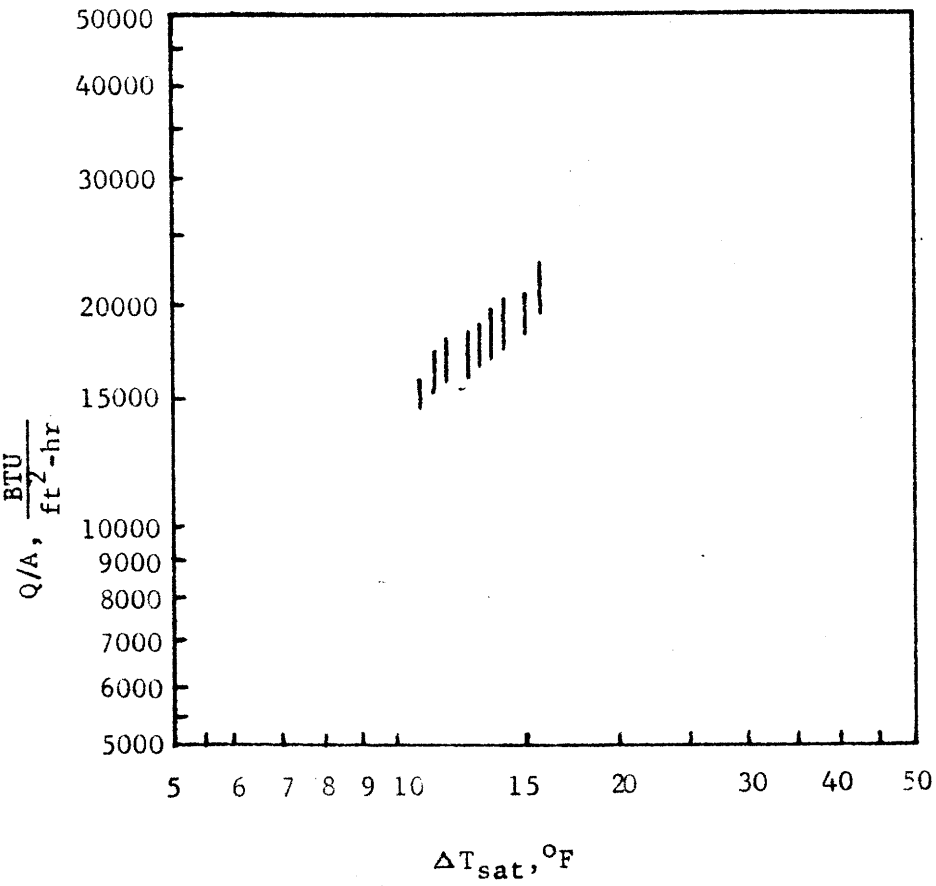

Fig. 7- Q/A versus ΔT_{sat} for water at atmospheric pressure

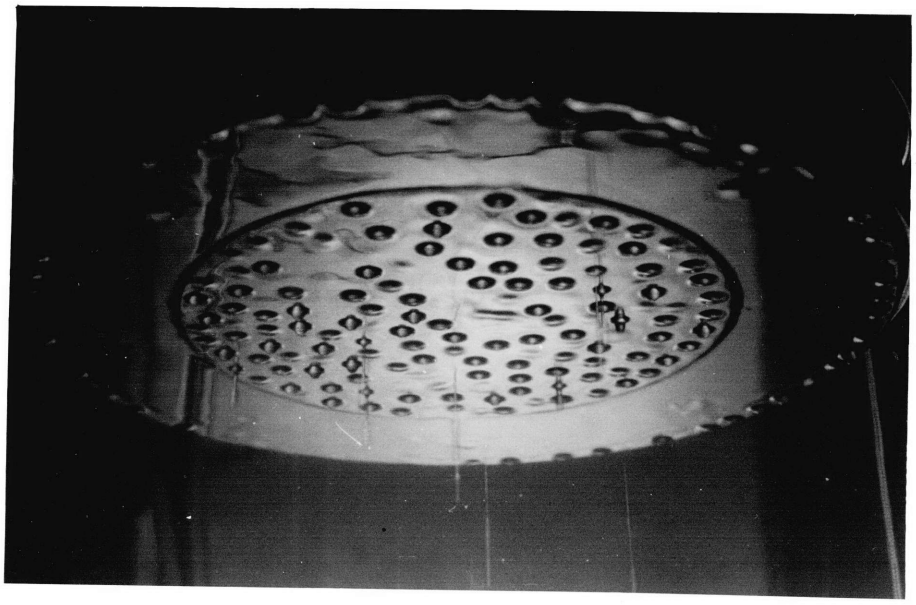

Freon 113 Condensing on a 5" Diameter Plate

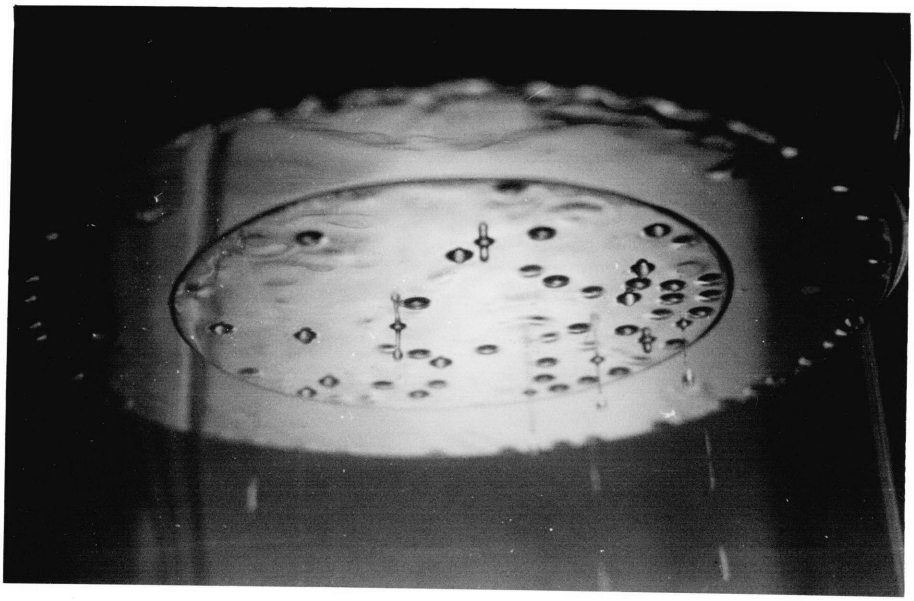

Freon 113 Condensing on a 5" Diameter Plate
with a Small Amount of Air Present

Figure 8

Figure 9 -Transient Drop Formation. Sequence spans about 20 Seconds

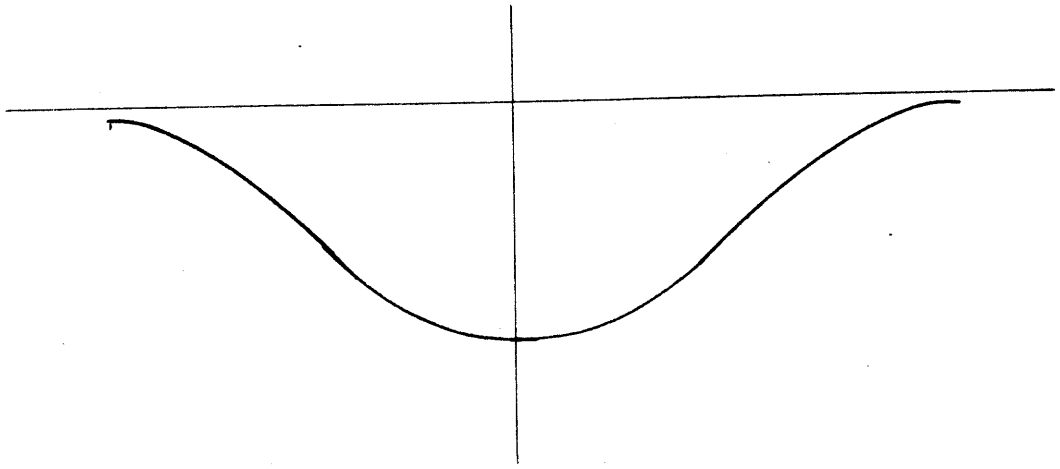

Fig.10a- Actual drop shape

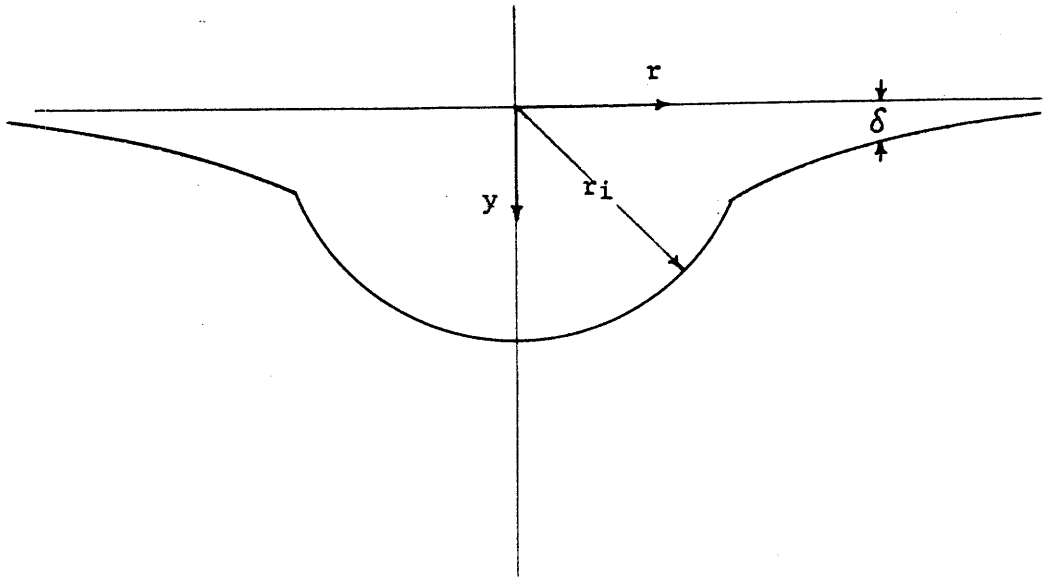

Fig. 10b- Assumed model of drop shape

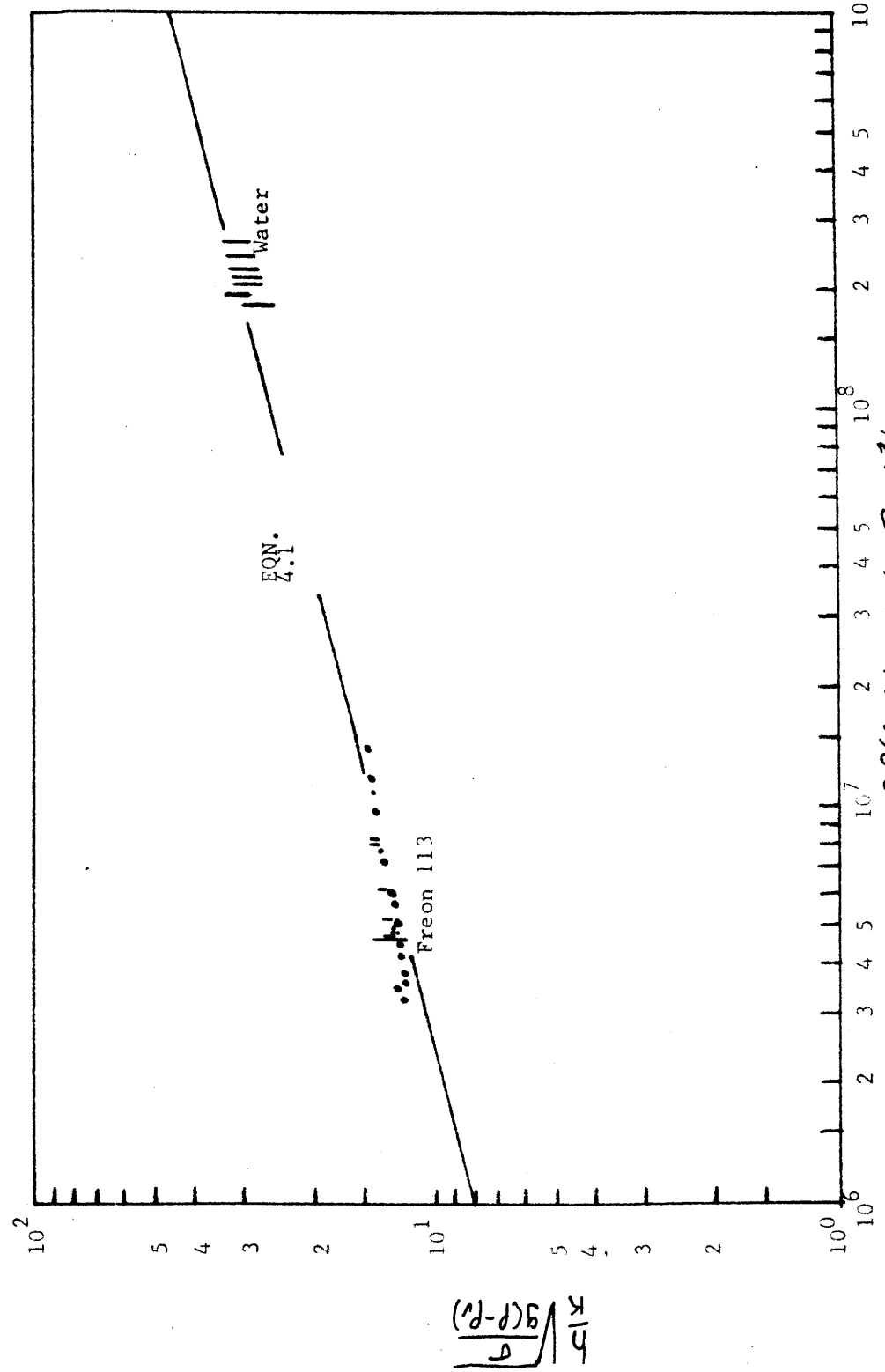

Fig. 11-Nusselt Number as a function of ΔT_{sat} for water and Freon 113